Communications Chemistry

https://doi.org/10.1038/s42004-025-01821-7

Article in Press

Advancing dye–DES synergies in dye-sensitized solar cells for improved indoor efficiency and long-term stability under sustainable conditions

Received: 12 May 2025

Accepted: 20 November 2025

Cite this article as: Salerno, G., Boldrini, C.L., Manfredi, N. *et al.* Advancing dye–DES synergies in dye-sensitized solar cells for improved indoor efficiency and long-term stability under sustainable conditions. *Commun Chem* (2026). https://doi.org/10.1038/s42004-025-01821-7

Giorgia Salerno, Chiara Liliana Boldrini, Norberto Manfredi, Vito Capriati, Ottavia Bettucci & Alessandro Abbotto

Advancing dye–DES synergies in dye-sensitized solar cells for improved indoor efficiency and long-term stability under sustainable conditions

Giorgia Salerno[1,2], Chiara Liliana Boldrini[1], Norberto Manfredi[1], Vito Capriati[3], Ottavia Bettucci[1], Alessandro Abbotto[1]**

[1] Department of Materials Science, Solar Energy Research Center MIB-SOLAR and INSTM Milano-Bicocca Research Unit University of Milano-Bicocca, Via Cozzi 55, I-20125, Milano, Italy.
[2] Department of Information and Electrical Engineering and Applied Mathematics (DIEM) University of Salerno, Invariante 12/B, Via Giovanni Paolo II, 132, Fisciano (SA) I-84084, Italy.
[3] Dipartimento di Farmacia–Scienze del Farmaco, Università degli Studi di Bari "Aldo Moro", Consorzio CINMPIS, Via E. Orabona 4, I-70125 Bari, Italy.

ottavia.bettucci@unimib.it, alessandro.abbotto@unimib.it

Two carbazole-based donor–acceptor dyes, CBZ-Gly and CBZ-EG, featuring glycerol- and ethylene glycol-like side chains, were designed and synthesized to achieve synergistic compatibility with DES-based electrolytes, and systematically investigate their impact on DSSCs performance. These dyes were tested in DSSCs employing two neat deep eutectic solvent (DES) electrolytes (choline chloride/ethylene glycol and choline chloride/glycerol) under both simulated sunlight (AM 1.5G) and indoor lighting (1000 lux). By combining molecular-level dye design with a tailored DES-based electrolyte, we achieved an improvement in long-term device stability over several months and demonstrated a record indoor power conversion efficiency of 9.4%, thereby establishing a new benchmark for fully sustainable, DES-based DSSCs under low-light conditions.

Introduction

In the last decade, the increasing demand for energy with net-zero greenhouse gas emissions has increased the focus on the full sustainability of renewable energy sources. To realize this vision, the integration of organic molecules into sustainable devices and as part of an experimental setup (i.e. photovoltaic (PV) devices,[1-6] photocatalytic setup for hydrogen production,[7-9] electro- and photocatalytic setup for ammonia production[10, 11]) is becoming a popular approach to get entire device's lifecycle greener.

Organic molecules can be synthesized from widely available and renewable resources, reducing reliance on rare or toxic materials often used in traditional energetic devices or catalysts. Additionally, molecular tunability and cost-effectiveness make organic molecules highly attractive for advancing sustainable energy technologies. Among all technologies, Dye-Sensitized Solar Cells (DSSCs), where the photoanode is typically a thin layer of TiO_2 sensitized by an organic dye, represent a promising green alternative to conventional solar energy technologies.[12] However, to reach good performances, the various components of a DSSC require simultaneous optimization. In particular, the electrolyte (typically, a redox pair such as I^-/I_3^-, Co^{2+}/Co^{3+}, or Cu^+/Cu^{2+} dissolved in a liquid medium)[13-15] presents significant challenges, as it is most of the time composed of a volatile organic compound (VOC). VOCs represent a major portion of industrial waste due to their toxicity, the high flammability, and the tendency to accumulate in the atmosphere,[16-18] thus, limiting the sustainability of the devices throughout their lifecycle. To overcome such issues, many studies are being conducted on the development of water-based electrolytes.[19-21] However, DSSCs are poorly stable in aqueous environments, as water hydrolyzes the ester-like bond between dye and semiconductor, causing fast dye desorption and the consequent device failure.[22, 23] To date, only one study reports an efficient stability up to 1 year of ambient light illumination of DSSC architecture using water-based electrolytes, reaching 9.3% efficiency under 1000 lux light.[24] Nevertheless, using water as

electrolyte medium in DSSC architectures is not immune to other drawbacks such as high energy consumption for purification, potential scarcity of water in some regions, and the limited solubility of most redox mediators.[20] Therefore, selecting green and biodegradable solvents that can both minimize the above-mentioned drawbacks and enhance device performances is essential for fostering a sustainable future.

In this context, Deep Eutectic Solvents (DESs), introduced in the early 2000s, have emerged as a good compromise between water and VOCs, due to their low volatility, high thermal stability, nonflammability, low cost, and customizable properties.[25] Additionally, DES-based electrolytes can help minimize the device's environmental impact due to their biodegradability and reusability. The first example of a DES-based DSSCs dates to 2009.[26] Since then, several studies from different groups, including our group, have been published investigating a significant number of DESs as electrolytes for DSSCs with remarkable results.[27-30] However, an interesting point still uncovered among the use of DESs in a DSSC architecture, lies in the interfacial interaction between the organic dye structure and the DES composition. The high compositional flexibility of DESs can indeed allow the fine-tuning of their physicochemical properties to match the dye structure and *vice versa*. To the best of our knowledge, only a few studies have demonstrated that the presence of hydrophilic pendants in the dye structure enhances the performance of DSSCs, likely due to improved interaction with the DES components.[27] Therefore, this topic remains largely unexplored and not fully rationalized. Moreover, to date, most electrolyte-based DESs are blended with water (from 5% to 40%) to improve fluidity, which compromises the long-term stability of DSSCs, making it another ongoing challenge.

The sustainable approach described above for the use and fabrication of DSSCs is also being extended to meet the demand for external energy to power indoor devices, whose number has dramatically increased with the growing reliance on technology, especially with the rise of the Internet of Things (IoT).[31] To mitigate such a trend, harvesting solar energy in indoor environments with DSSCs, exploiting properly designed organic dyes, is becoming popular offering a sustainable energy solution for everyday applications.[15, 20, 32-35] DSSCs can indeed operate efficiently under lower light conditions, where other solar technologies struggle, thanks to their higher ability to diffused-light catching. Moreover, they offer design tunability, including transparency and flexibility in structure, which enhances their integration into indoor environments.[12, 36-38] Unlike traditional silicon-based cells, DSSCs can be tailored by selecting specific organic dyes that match the emission spectrum of indoor light sources allowing them to optimize their energy harvesting capabilities.[39] This capability positions DSSCs ahead of other technologies. Indeed, despite advancements in the tunability of perovskites (PSCs) and organic solar cells (OSCs) which achieved efficiencies of up to 32.6%[40-43] and 33%[44] under 1000 lux illumination, DSSCs still represent a valuable alternative for indoor energy harvesting applications, offering additional advantages also in terms of material, production costs and long-term stability.

However, compared with outdoor applications, in indoor environments safety requirements must be even more stringent regarding the use of VOCs, to reduce the risk in the case of leakages or accidental breakage. So, despite the efficiency record of 38% obtained for VOC-based DSSC under ambient light,[45] the replacement of VOCs with safer, environmentally friendly solvents cannot be postponed. So far, only one paper from our group explored the possibility of using a DES-like mixture (choline iodide/ethylene glycol (ChI:EG) in a DSSC architecture under indoor lighting conditions (1200 lux, OSRAM 765 fluorescent lamp) achieving 8% efficiency.[46]

To fill this knowledge gap, and overcome all the above-mentioned issues, we investigated two DESs – choline chloride/ethylene glycol (ChCl:EG) and choline chloride/glycerol (ChCl:Gly), both in a 1:2 molar ratio – as neat electrolytes, without the addition of water, in DSSCs. Moreover, the DSSCs have been sensitized with two dyes, CBZ-EG and CBZ-Gly, properly

designed and synthesized to introduce an ethylene glycol-like and a glycerol-like pendant, respectively, to investigate the effect of matching the hydrophilic pendants of the dye with the hydrophilic portion of the DES on the DSSCs performances (Figure 1). The main π-framework of the dyes originates from our design of dibranched donor–π–acceptor dyes, which we introduced a few years ago[47] and which have since been adopted by many other researchers.[48] These dyes have been thoroughly investigated both in DSSC applications and in the photogeneration of green hydrogen. The donor core is based on a carbazole moiety, which is particularly suitable for terminal functionalization through its nitrogen atom. A thiophene unit serves as the π-spacer, while the commonly used cyanoacrylic acid functions as the electron acceptor and anchoring group for TiO_2. To validate the dye-DES matching assumption, a reference compound CBZ-Alk (bearing a simple alkyl chain as a pendant) has also been synthesised (Figure 1). Through this study it has been possible to increase DSSCs stability and devices performances both under AM 1.5G 1 sun-simulated light (outdoor conditions) and under 1000 lux (indoor conditions) using two different lamps: OSRAM 930 (warm light T8 fluorescent lamp, OSRAM L 18 W/930) and OSRAM 765 (cold light T5 fluorescent lamp – OSRAM L 8 W/765). The selected fluorescent light sources were chosen for their widespread use in indoor environments, their large adoption in DSSC literature[24,34,39,45,46] and their distinct spectral profiles, which allow for meaningful comparison with dye absorption characteristics.[39] This work demonstrates that by carefully designing the dye-sensitizer adjusting its nature and properly matching the electrolyte characteristics, it is possible to foster a synergistic relationship between semiconductor and electrolyte, thereby improving the performance of the devices.

Results and Discussion

Synthesis of CBZ-Based Organic Sensitizers

The reference compound CBZ-Alk was synthesized following a previously reported procedure.[49] The dyes, CBZ-EG and CBZ-Gly, have been obtained through an accurate optimization of experimental conditions. Both syntheses were carried out by synthesizing the building blocks **1a,b**[50, 51] and **2a,b**[52] under the conditions reported in the literature. The two products were then submitted to a nucleophilic substitution to afford *N*-alkylation of the carbazole terminal unit to obtain the products **3a,b**. Compound **3a** has been then brominated to obtain product **4b.** To introduce the thiophene π-spacer into the structure, product **3a** and **4b** have been functionalized through a Suzuki-Miyaura cross-coupling with 5-formyl-2-thiopheneboronic acid (**5**). The obtained dialdehydes (**6a,b**) were then converted into the corresponding diacid **7a,b** through the commonly adopted Knoevenagel condensation with cyanoacetic acid, allowing isolation of the desired products in high yields. To obtain the final product, CBZ-EG and CBZ-Gly, a deprotection in acidic conditions was carried out to give both dyes in high yield. All the details about compound preparation and synthetic pathways are shown in Scheme 1 and in the Supplementary Methods (pages 2-4). All the intermediates have been investigated by ^{1}H-NMR spectroscopy, while the two dyes CBZ-EG and CBZ-Gly have been characterized in detail (Supplementary Methods pages 2-4 and Figure 1-4).

Optical and Electrochemical Investigation of Dyes

To validate the suitability of the dyes in a DSSC configuration, spectroscopic and electrochemical characterization have been carried out. The UV-Vis spectra of all dyes recorded in THF (Supplementary Figure 5a) present an intense intramolecular charge-transfer (ICT) band in the 350 – 550 nm region and a molar extinction coefficient (ε) in the range of

30000 - 40000 ($M^{-1}\,cm^{-1}$) according to the literature data reported for the reference dye CBZ-Alk (Supplementary Table 1).[53] When adsorbed on transparent TiO_2 films (P25, approximately 1-μm thick), compounds showed slightly blue-shifted absorption maxima compared to those recorded in solution and a dramatic broadening of the absorption bands (Supplementary Figure 5b). This common behavior can be due both to deprotonation following adsorption on the semiconductor surface and formation of blue-shifting H-aggregates.[54] Although this absorption range does not fully cover the emission spectrum of all indoor light sources (e.g., LEDs extending up to ca. 700 nm), the dyes were purposely designed based on a robust donor–π–acceptor scaffold optimized for DES-based DSSCs and for compatibility with the fluorescent lamps used in this work, as well as with commonly adopted indoor fluorescent lighting. Optical bandgap has been evaluated by means of Tauc plots.[55] The Cyclic Voltammetry (CV) of the dyes, recorded in CH_2Cl_2 $TBABF_4$ 0.1 M solution, showed a non-reversible or a quasi-reversible behavior at oxidative potentials (potential > 0 V vs. Fc/Fc+) (Supplementary Figure 6a). Upon this behavior, since the $E_{1/2}$ evaluation in case of not reversible peaks is not possible, Differential Pulse Voltammetry (DPV) (Supplementary Figure 6b) was preferred to determine the oxidation (E_{ox}) potentials and, thus, to calculate the HOMO energy levels (Supplementary Table 1). The calculated LUMO level for all dyes (estimated from the corresponding HOMO energy and the optical bandgap) appears adequate for allowing efficient electron injection into the conduction band (CB) of the TiO_2-based catalyst (all calculated values are listed in Supplementary Table 1).[55] Moreover, the ca. 2.2 eV bandgap ensures effective spectral matching with the OSRAM 765 and OSRAM 930 lamps as well as with the LED B4 emission range (450–630 nm), supporting their potential applicability under standardized indoor LED conditions, although LED B4 was not directly employed in this study, but it is widely used as a standard indoor light source in DSSC benchmarking.

Photovoltaic Properties under AM 1.5G irradiation

Upon complete characterization of the three dyes, DSSCs were fabricated using two different DES-based electrolytes: ChCI:EG and ChCl:Gly, both in a 1:2 molar ratio. DES-based electrolytes have been prepared mixing the DES in the presence of 1-methyl-3-propylimidazolium iodide (PMII) as a conventional iodide source following the formulation reported in the literature.[27] *J/V* and IPCE curves of DSSCs functionalized with dyes CBZ-EG, CBZ-Gly and CBZ-Alk (recorded at 1 sun, AM 1.5G), filled with either ChCI:EG or ChCl:Gly based electrolytes, are depicted in Figure 2 and 3. In Figure 2 a,b the *J/V* curves of the DSSCs sensitized by CBZ-based dyes showed a different trend depending on the used DES electrolyte. In the presence of ChCl:EG based electrolyte (Figure 2a, blue panel), the best-performing device results to be the one sensitized with CBZ-EG, reaching a PCE of 2.0%, while the one sensitized with CBZ-Gly exhibited lower performance (PCE of 1.7%). An opposite behavior was observed when ChCl:Gly based electrolyte is used (Figure 2b, green panel). Here, the DSSC sensitized with CBZ-Gly outperformed the other devices, reaching a PCE of 3.0% vs. 1.55% of CBZ-EG sensitized cells. As further evidence of the crucial role of the dye-DES interaction, when CBZ-Alk was used as a sensitizer, a lower performance in both DES-based electrolytes has been observed (0.9% with ChCl:EG and 0.7%, with ChCl:Gly). In Figure 3a,b the incident photon-to-current efficiency (IPCE) curves of DSSCs with the two different DES-based electrolytes are shown. For all the investigated devices, IPCE curves resemble the UV-vis absorption spectrum of the corresponding sensitizer shifted towards lower energies. The shape of the curves is similar in the different electrolyte solutions, with a wide absorption up to ca. 650 nm and a maximum at ca. 490-510 nm. The trend of IPCE curves is consistent with the performance of the cells. In particular, the highest IPCE value has been recorded for the cell sensitized by CBZ-Gly containing ChCl:Gly-based electrolyte solution, with a peak of ca. 70%. Moreover, the integrated photocurrent calculated from the IPCE spectra well matches the value recorded for the corresponding cells measured under AM1.5G conditions with a black mask on top

(Supplementary Table 2). All photovoltaic characteristics are listed in Table 1. To further understand the behavior of the dyes under standard conditions, a comparative study was carried out using two conventional acetonitrile-based electrolytes (I^-/I_3^- and $Cu^{(II/I)}(tmby)_2TFSI_{(1/2)}$) (Supplementary Figure 8 and Table 3). The photovoltaic performances obtained with such electrolytes are consistent with literature values for similar systems, confirming the reliability of the developed dyes.[56,57] Interestingly, when using organic solvent-based electrolytes, a different trend in performances is observed: in this case, CBZ-Alk exhibits the highest efficiency, reaching a PCE of 3.2% with I^-/I_3^- and 2.9% with $Cu^{(I/II)}(tmby)_2TFSI_{(1/2)}$. This result supports our hypothesis regarding the critical role of dye-electrolyte compatibility. The superior performance of CBZ-Alk in conventional electrolytes likely arises from its greater molecular affinity with acetonitrile-based environments, whereas CBZ-Gly and CBZ-EG are favored in DES-based devices. Overall, this comparative analysis provides an additional validation of our design strategy, highlighting the importance of optimizing dye-electrolyte composition for each specific medium.

Electrochemical Impedance Spectroscopy Analysis of Charge-Recombination Pathways

For a deeper analysis of the interfacial processes occurring at the electrode surface induced by the dye-DES interaction, charge-recombination dynamics have been investigated by means of Electrochemical Impedance Spectroscopy (EIS). EIS experiments, on the best-performing cells under 0.23 sun AM1.5G illumination, were performed by applying a small sinusoidal voltage stimulus to the solar cell at the V_{oc} potential, while measuring the current response. By changing the frequency over several orders of magnitude (from mHz to MHz) it is possible to study the behavior of the device. EIS spectra are depicted as Nyquist plots, where the imaginary part of the impedance is reported as a function of the real part (Figure 4). The Nyquist plot can be fitted by a proper equivalent circuit, leading to important information like the recombination resistance (R_{rec}) and the chemical capacitance (C_μ), which allow the calculation of the electron lifetime τ_n as: $\tau_n = R_{rec} \times C_\mu$.[58-60] Nyquist plots of the investigated cells under light are depicted in Figure 4 and the corresponding fitting parameters are listed in Table 2. The electron lifetimes well match the trend in V_{oc} of the investigated devices. In particular, the chemical capacitance of cells filled with ChCl:EG solution is lower than with ChCl:Gly whichever the dye and is very similar among the different devices. The biggest difference thus lies in the recombination resistance, which indeed depends on the interactions at the interface between the sensitised TiO_2 and the electrolyte solution. The highest R_{rec} corresponds to the dye that better reflects the DES composition, namely CBZ-EG in ChCl:EG cells and CBZ-Gly in ChCl:Gly filled cells. Due to the higher chemical capacitance, devices filled with ChCl:Gly DES result in higher electron lifetimes, well matching the higher V_{oc} recorded with the same dye with this electrolyte. Such study also justifies the relatively low fill factors obtained in some conditions that can be attributed to redox mediator kinetics, interfacial recombination, and charge transport limitations. All results obtained confirm our assumption that increased affinity between the dye structure and the DES composition ensures a synergistic effect, which influences the charge transfer dynamics with a consequent higher power conversion efficiency.

Temporal Stability of CBZ-DSSCs with neat and aqueous DES electrolytes

A proper dye-DES matching could also help stabilize the dye in its adsorbed state on the semiconductor surface, reducing desorption and improving long-term device stability. To validate this hypothesis, the long-term stability of DSSCs with the best-performing DES electrolyte – neat ChCl:Gly– was evaluated over a period of four months of DSSCs (Figure 5). In Figure 5a-i,ii, it is possible to observe the variation in PCE and J_{sc} values of the three DSSCs

sensitized by CBZ-based dyes over 120 days. Both devices sensitized with CBZ-EG and CBZ-Gly showed excellent stability of PCE and J_{sc} values throughout the experiment. The PCE values in both cases remained stable around 2.6% for CBZ-Gly and 1.5% for CBZ-EG. In contrast, the device sensitized with CBZ-Alk showed a drop of PCE after 20 days (Figure 5a-ii), which dramatically decreased to zero by the end of the experiment. Similarly, the J_{sc} dropped to less than 1 mA after 30 days, decreasing to almost zero by the end of the experiment. This different behavior is even more evident in Figure 5b, where the *J/V* curves of the dyes at day 1 and at day 120 are shown. In Figure 5b-i, ii DSSCs sensitized with CBZ-EG and CBZ-Gly maintained the expected diode-like *J/V* curve over all the monitored time. In contrast, CBZ-Alk-based DSSCs at day 120 showed a quasi-resistive behavior with almost zero current, meaning the device was no longer working (Figure 5b-iii). On the other hand, these results confirm the previous assumption that a beneficial dye-DES matching can help stabilize the dye in its adsorbed state on the semiconductor surface, improving long-term device stability. Variations of all parameters are collected in the Supplementary Table 4 while the variation of FF and V_{oc} over the time are shown in the Supplementary Figure 8. Another key aspect of this work is the use of neat DES electrolyte, in contrast to the more common water-diluted DES systems reported in the literature. Typically, water is added - often up to 40% w/w[27, 61, 62] - to reduce viscosity, and facilitate the electrolyte intercalation into the semiconductor layer.[19, 63] However, this common practice compromises the long-term stability of the devices, often leading to dye desorption from the semiconductor surface. For this reason, a comparative study was conducted in this work between DSSCs sensitized with CBZ-based dyes using either a neat DES electrolyte or a water-containing DES electrolyte (40% w/w), in order to evaluate the impact of water dilution on device performance (Figure 6). In Figure 6a the *J/V* curves of DSSCs sensitized by CBZ-based dyes using the best performing DES electrolyte (ChCl:Gly) in the presence or absence of water showed different results depending on the dye used. For DSSCs sensitized with CBZ-Gly, a dramatic loss in PCE values has been observed when the water-based DES electrolyte was used, with an efficiency drop from 3 to 1% (Figure 6a blue solid and dotted lines). Such PCE decrease can be attributed to the loss of the optimal interaction between the hydrophilic components of the dye and DES which led to an improved stability and reduced desorption when the DES was pure. Conversely, when CBZ-EG was used as a sensitizer, PCE remained almost the same exhibiting efficiency values of 1.6% with pure DES and 1.5% with aqueous DES (Figure 6a pink solid and dotted lines). Finally, for the CBZ-Alk-based DSSC, a slight improvement was seen, reaching 1.0% in aqueous DES compared to 0.7% in pure DES (Figure 6a green solid and dotted lines). The slight improvement observed with the CBZ-Alk can be rationalized by the hydrophobic chain protection of semiconductor reducing TiO_2-electrolyte recombination.[64] Such behavior highlights a key point to support our thesis: when water is added to the DES, the interfacial stability induced by the match between the hydrophilic nature of the dye and the DES is lost. The stability of the DSSCs sensitized by CBZ-based dyes containing the aqueous DES electrolyte was also tested over 30 days and the variation of PCE and J_{sc} values has been monitored over the time (Figure 6b-i,ii). Such test showed a dramatic drop to zero in PCE (and consequently in J_{sc}) for CBZ-EG and CBZ-Alk just after 20 days and a slightly slower decrease of both parameters for CBZ-Gly. However, for all devices a decrease to almost zero of both parameters has been observed by the end of the experiment (Figure 6b-i,ii). These results well align with studies reported in the literature,[63, 65] confirming the poor stability of DSSCs in the presence of water, and highlights that the use of pure DES electrolyte, combined with the proper functionalization of the dye, improves the long-term stability of the device. All photovoltaic data are collected in Table 3 while the variation of all photovoltaic parameter over 30 days is listed in Table S5. Variation of V_{oc} and FF over the time are shown in Supplementary Figure 10.

Photovoltaic Properties Under Indoor Lighting (1000 lux)

After these encouraging results obtained under conventional AM 1.5G sun-simulated light, the three DSSCs sensitized by CBZ-based dyes were tested under low light conditions (1000 lux). Two commonly used indoor light sources have been adopted: a warm light T8 fluorescent lamp (OSRAM 930) and a cold fluorescent lamp (OSRAM 765).[12, 34, 39] The choice of the two lamps was based on common representative indoor lighting sources usually found in indoor settings and frequently reported in the literature. Moreover, the chosen lamps exhibit different emission profiles allowing an investigation about the relationship between CBZ-dye absorption and the lamp's emission profile and its effect on DSSC performances.

As demonstrated in one of our recent works, the overlap between the dye absorption profile and the lamp emission profile allows the calculation of a parameter, called "*f*" factor, which estimates the goodness of the dye-lamp matching.[39] As shown in Supplementary Figure 11, the absorption spectra of all dyes cover a better portion of the OSRAM 765 lamp emission profile than those of OSRAM 930. The qualitative spectra analysis has been then confirmed by the calculated *f* factors which result to be 20 - 30 times higher than those obtained with the OSRAM 930 lamp (Supplementary Figure 12 and Supplementary Table 6) in agreement with the literature.[39] This better coverage of the lamp emission spectrum is confirmed by DSSC performances: indeed, PCE values with both electrolytes were significantly higher when OSRAM 765 was used (Table 3).

As expected, a behavior similar to that showed under 1 sun illumination was also observed under indoor lighting conditions. The proper combination of the dye hydrophilic pendant and the hydrophilic component of the DES also in this case induces an increase in DSSC performance also in indoor settings. When ChCl:EG was used as the electrolyte (Supplementary Figure 13a, blue panel), the DSSC sensitized with CBZ-EG was the best-performing device, reaching a PCE value of 6% (see Table 3).

Even more remarkably, when ChCl:Gly was used as an electrolyte (Supplementary Figure 13b, green panel), the devices sensitized with CBZ-Gly achieved a new efficiency record of 9.4%, reaching the highest performance ever among DES-based DSSCs under indoor conditions (Table 3). The same trend was observed when OSRAM 930 was used, although the differences were less pronounced compared to the results obtained with OSRAM 765 (Supplementary Figure 14). This can be easily explained by the previously mentioned weaker overlap between the lamp's emission profile and the dyes absorption spectra (Supplementary Figure 11), which led to a decrease in DSSC performances in agreement with the literature.[39] All photovoltaic data obtained under OSRAM 765 illumination and under OSRAM 930 are summarized in Supplementary Table 7 and 8, respectively. To complement the indoor performance analysis under DES-based electrolytes, *J/V* curves were recorded for the same CBZ-sensitized DSSCs using conventional acetonitrile-based electrolytes (I^-/I_3^- and $Cu^{(II/I)}(tmby)_2TFSI_{(1/2)}$) under the best-performing indoor illumination conditions (OSRAM 765, 1000 lux), as shown in Supplementary Figure 15 and Supplementary Table 9. Similarly, to what observed under AM 1.5G conditions**,** the previously observed PCE trend was not preserved. CBZ-Alk exhibited slightly superior efficiencies reaching a PCE of 8.2% with both I^-/I_3^- and $Cu^{(II/I)}(tmby)_2TFSI_{(1/2)}$. The relatively improved behavior of CBZ-Alk in conventional electrolytes can be attributed to its higher compatibility with acetonitrile-based media, consistent with the trends observed under 1 sun illumination. This recurring behavior across both standard and indoor conditions provides additional validation of our hypothesis on the importance of dye–electrolyte matching as a guiding principle in the design of efficient and tunable DSSC systems for different operating environments.

All these findings highlight the strong potential of DES-based DSSCs as a competitive and sustainable solution for indoor photovoltaics. While their absolute efficiencies remain lower than those of organic solvent-based DSSCs and other photovoltaic technologies (e.g., PSCs or OSCs), the combination of high chemical stability, low toxicity, absence of volatile solvents, and extended device lifetime under real-world conditions positions them as a highly promising

technology for safe, cost-effective, and environmentally conscious energy harvesting. In particular, the excellent operational stability observed in our devices further reinforces the suitability of DES electrolytes for long-term indoor applications, where durability and reliability are crucial performance metrics.

Conclusions

In this study, two dyes bearing hydrophilic side chains (CBZ-EG and CBZ-Gly) were successfully synthesized to investigate their synergistic interplay with the hydrophilic nature of two selected DES-based electrolytes within a DSSC architecture.

DSSCs sensitized by CBZ-Gly and filled with a neat ChCl:Gly-based electrolyte achieved a PCE of 3.0% under standard 1 sun conditions. Beyond performance enhancement, long-term stability tests demonstrated that the combination of neat DES electrolytes with well-matched hydrophilic dyes plays a crucial role in preserving device durability over a four-month period. Additionally, this study explored DSSC performance under indoor lighting conditions, where the interplay between dye absorption and lamp emission spectra was investigated. Our findings validated the dye-lamp matching hypothesis, showing that the overlap between the dye absorption profile and the light source spectrum significantly influences device efficiency. Under OSRAM 765 illumination, DSSCs sensitized by CBZ-Gly, and employing a neat ChCl:Gly electrolyte, achieved a record indoor PCE of 9.4% among DSSC devices based on eco-friendly components, such as DESs. Given its outstanding efficiency and proven long-term stability, the CBZ-Gly-sensitized DSSC represents, to the best of our knowledge, the most efficient DES-based DSSC reported to date for indoor applications. Overall, this work underscores the importance of rational dye design and electrolyte selection in significantly enhancing DSSC performance.

Methods

General information. The starting reagents, obtained from commercial suppliers at the highest purity grade, were used without further purification. Anhydrous solvents and all commercial compounds have been sourced from Sigma-Aldrich and were used as received. Extracts were dried with Na_2SO_4, filtered, and the solvent was removed by evaporation. FTO-coated glass plates and Dyesol 18NR-T titania pastes were purchased from commercial suppliers. UV-O_3 treatment was conducted using a Novascan PSD Pro Series-Digital UV Ozone System. Layer thickness was measured with a VEECO Dektak 8 Stylus Profiler. UV–vis spectra were acquired using a Jasco V-570 spectrophotometer, while NMR spectra were recorded on a Bruker Advance-Neo spectrometer operating at 400 MHz. Electrochemical measurements were performed using a Bio-logic SP-240.

DES preparation. Deep eutectic solvents such as ChCl:Gly and ChCl:EG (both in a 1: 2 mol/mol ratio) were prepared by gently heating the respective components at 60–80 °C under continuous stirring for 10–50 min, until a homogeneous and transparent solution was obtained.

DES-electrolyte solution. The electrolyte solution was prepared at room temperature by mixing 1 mL of the eutectic mixture ChCl:EG or ChCl:Gly (1:2 mol/mol) with iodine (20 mM) and PMII (2 M). The resulting mixture was sonicated for 10 min, kept in the dark under ambient air, and used within one week of preparation.

VOCs-electrolyte solution. The I^-/I_3^- electrolyte solution was prepared at room temperature by mixing in acetonitrile 0.1 M LiI, 0.6 M TBAI, 0.05 M I_2 and 0.5 M 4TBP. The resulting mixture was sonicated for 10 min, kept in the dark under ambient air, and used within one week of

preparation. The $Cu^{(II/I)}(tmby)_2TFSI_{(1/2)}$ electrolyte solution was prepared at room temperature by mixing in acetonitrile 0.1M LiTFSI and 0.6 M of 4TBP and 0.2 M $Cu^{(I)}(tmby)_2TFSI$ and 0.04 $Cu^{(II)}(tmby)_2TFSI_2$. The resulting mixture was sonicated for 10 min, and kept in the dark.

DSSC fabrication procedure. DSSCs have been prepared by adapting a procedure reported in the literature.[66] To exclude metal contamination, all the containers were glass or Teflon and were treated with EtOH and 10% HCl before use. Plastic spatulas and tweezers have been used throughout the procedure. FTO glass plates were cleaned in a detergent solution for 15 min using an ultrasonic bath, rinsed with pure water and cleaned again for 15 min in an ultrasonic bath with EtOH. After treatment in a UV–O_3 system for 18 min, the FTO plates were treated with a freshly prepared 40 mM aqueous solution of $TiCl_4$ for 30 min at 70 °C, rinsed with water and EtOH and heated at 500 °C for 30 min. A transparent layer of 0.20 cm^2 was screen-printed using a 20 nm transparent TiO_2 paste (Dyesol 18NR-T). The coated films were thermally treated at 125 °C for 5 min, 325 °C for 10 min, 450 °C for 15 min, and 500 °C for 15 min. The heating ramp rate was 5–10 °C min^{-1}. The sintered layer was treated again with 40 mM aqueous $TiCl_4$ (70 °C for 30 min), rinsed with EtOH and heated at 500 °C for 30 min. After cooling down to 80 °C, the TiO_2 coated plate was immersed in a 0.2 mM solution of the dye for 18 h at room temperature in the dark. PEDOT counter electrodes were prepared according to the following procedure[67]: a 1 mm hole was made in a FTO plate using diamond drill bits. Then the electrodes were cleaned with a detergent solution for 15 minutes using an ultrasonic bath, 10% HCl, and finally acetone for 15 min using an ultrasonic bath. Then the electrodes were manufactured via electro-polymerization of 3,4-ethylenedioxythiophene from 0.01 mM aqueous solution with 0.1 M sodium dodecyl sulphate, as reported in the literature. The dye-adsorbed TiO_2 electrode and the counter electrode were assembled into a sealed sandwich-type cell by heating with hot-melt ionomer-class resin (Surlyn 30 μm thickness) as a spacer between the electrodes. The same configuration was used for symmetrical dummy cells consisting of two identical PEDOT counter electrodes working, respectively, as the anode and cathode. The electrolyte solution was prepared by mixing at room temperature 20 mM I_2 and 2 M PMII in ChCl:EG or a ChCl:EG 1: 2 DES-like mixture and kept in the dark in air. A drop of the electrolyte solution was placed over the hole and introduced inside the cell by vacuum backfilling. Finally, the hole was sealed with a sheet of Surlyn and a cover glass.

DSSC measurements (1.5 AG, simulated sunlight). PV measurements of DSSCs were carried out under a 550 W xenon light source (ABET Technologies Sun 2000 class ABA Solar Simulator) with a thermostatic stage at 36 °C. The power of the simulated light was calibrated to AM 1.5G (100 mW cm^{-2}) using a reference Si cell photodiode equipped with an IR-cutoff filter (KG-5, Schott) to reduce the mismatch in the region of 350–750 nm between the simulated light and the AM 1.5G spectrum.

DSSC measurements (1000 lux, low light condition). Indoor-light curves were obtained using two different light sources: a cold light T5 fluorescent lamp (OSRAM L 8W/765, abbreviated as OSRAM 765) and a warm white, fluorescent tube (OSRAM 930 18 W, abbreviated as OSRAM 930). The light source was placed at a distance such as to illuminate the surface of interest with an illuminance equal to 1000 ± 50 lux. Illuminance was determined from the irradiance spectra of the lamps. The emission spectrum of the light sources in the wavelength range from 300 to 1000 nm was measured by using a Hamamatsu C10082CAH spectrophotometer and a power meter (Thorlabs PM100USB power and energy meter) equipped with a photodiode calibrated for the purpose (Si-photodiode S120VC, recalibrated in March 2023 by ReRa Solutions). Figure 2c and 2d show the spectral distribution of the irradiance (power per unit illuminated area at the distance of interest). The photodiode was

used to continuously check the power of the lamp before measuring the *J/V* curve of each cell. The entire active photovoltaic area of the devices was used during indoor characterization to mimic diffuse light conditions. The measurements were performed at room temperature (24 ± 1 °C). In both cases, *J/V* curves were obtained by applying an external bias to the cell and measuring the generated photocurrent with a Keithley model 2440 digital source meter. For each combination of dye/electrolyte, multiple cells have been prepared and tested for average values of 3 independent cells. Values, including standard errors, are presented in Table S6, S7. Incident photon-to-current conversion efficiencies (IPCEs) were recorded as a function of excitation wavelength by using a monochromator (Omni 300 LOT ORIEL) with a single grating in Czerny–Turner optical design, in AC mode with a chopping frequency of 1 Hz, applying a 0.3 sun halogen lamp bias, at room temperature (24 ± 1 °C).

Electrochemical Impedance spectroscopy (EIS). EIS spectra were obtained using a Bio-logic SP-240 galvanostat potentiostat. The measurements have been performed in the frequency range from 100 kHz to 20 mHz under AC stimulus with 10 mV amplitude, under 0.23 sun solar irradiation at the open circuit voltage at 36 °C.[68,69] The obtained Nyquist plots have been fitted *via* a non-linear least-squares procedure using the equivalent circuit model depicted in the inset of the plot itself.

Electrochemical characterization. Cyclic Voltammetry (CV) was carried out at a scan rate of 100 mV s^{-1}, using a Bio-logic SP-240 potentiostat in a three-electrode electrochemical cell under nitrogen. The working, counter, and the pseudo reference electrodes were an FTO working electrode (surface area = 1 cm^2), an Ag/Ag^+ TBAP in CH_3CN (0.1 M tetrabutylammonium perchlorate and 0.01 M $AgNO_3$ in acetonitrile) and a Pt wire in a 0.1 M $TBABF_4$ solution in CH_2Cl_2. The same setup was used for Differential Pulsed Voltammetry (DPV), recorded at a scan speed of 12.5 mV s^{-1} and a pulse height of 50 mV. The Pt wire was sonicated for 15 min in deionized water, washed with 2-propanol, and cycled for 50 times in 0.5 M H_2SO_4 before use. The Ag/Ag^+ pseudo-reference electrode was calibrated by adding ferrocene (10^{-3} M, Fc) to the test solution after each measurement.

Synthetic procedures. The synthetic procedures for the preparation of the CBZ-dyes are presented in Supplementary Methods pages 2-4.

Data availability

The authors declare that all data supporting the findings of this study are available within the paper and its supplementary information files

References

1 Gao, W. *et al.* Efficient all-small-molecule organic solar cells processed with non-halogen solvent. *Nat. Commun.* **15**, 1946, (2024).

2 Zhou, R. *et al.* All-small-molecule organic solar cells with over 14% efficiency by optimizing hierarchical morphologies. *Nat. Commun.* **10**, 5393, (2019).

3 Prajapat, K. *et al.* The evolution of organic materials for efficient dye-sensitized solar cells. *J. Photochem. Photobiol. C: Photochem. Rev.* **55**, 100586, (2023).

4 Bettucci, O. *et al.* Dendritic-Like Molecules Built on a Pillar[5]arene Core as Hole Transporting Materials for Perovskite Solar Cells. *Chem. Eur. J.* **27**, 8110-8117, (2021).

5 Gatti, T. *et al.* A D-π-A organic dye – Reduced graphene oxide covalent dyad as a new concept photosensitizer for light harvesting applications. *Carbon* **115**, 746-753, (2017).

6 Bettucci, O. *et al.* Tailoring the Optical Properties of Organic D-π-A Photosensitizers: Effect of Sulfur Introduction in the Acceptor Group. *Eur. J. Org. Chem.* **2019**, 812-825, (2019).

7 Salerno, G. *et al.* Enhanced Long-Term Stability of a Photosensitizer with a Hydroxamic Acid Anchor in Dye-Sensitized Photocatalytic Hydrogen Generation. *Eur. J. Org. Chem.* **26**, e202300924, (2023).

8 Liu, S. *et al.* Promotion of photocatalytic hydrogen production by utilization of triplet excited states of organic dyes and adjustment of π–π interactions. *J. Mater. Chem. A* **11**, 14682-14689, (2023).

9 Chen, Y. *et al.* Improving Photocatalytic Hydrogen Production through Incorporating Copper to Organic Photosensitizers. *Inorg. Chem.* **61**, 12545-12551, (2022).

10 Bettucci, O., Salerno, G., Manfredi, N. & Abbotto, A. Molecular electro- and photocatalytic approach to artificial nitrogen fixation for the synthesis of green ammonia. *Tetrahedron Green Chem.* **3**, 100040, (2024).

11 Salerno, G. *et al.* Tailored Metal-Porphyrin Based Molecular Electrocatalysts for Enhanced Artificial Nitrogen Fixation to Green Ammonia. *Global chall.* **8**, 2300345, (2024).

12 Muñoz-García, A. B. *et al.* Dye-sensitized solar cells strike back. *Chem. Soc. Rev.* **50**, 12450-12550, (2021).

13 Feldt, S. M. *et al.* Design of Organic Dyes and Cobalt Polypyridine Redox Mediators for High-Efficiency Dye-Sensitized Solar Cells. *J. Am. Chem. Soc.* **132**, 16714-16724, (2010).

14 Kakiage, K. *et al.* An achievement of over 12 percent efficiency in an organic dye-sensitized solar cell. *Chem. Commun.* **50**, 6379-6381, (2014).

15 Zhang, D. *et al.* A molecular photosensitizer achieves a V(oc) of 1.24 V enabling highly efficient and stable dye-sensitized solar cells with copper(II/I)-based electrolyte. *Nat. Commun.* **12**, 1777, (2021).

16 Clarke, C. J., Tu, W.-C., Levers, O., Bröhl, A. & Hallett, J. P. Green and Sustainable Solvents in Chemical Processes. *Chem. Rev.* **118**, 747-800, (2018).

17 Lipshutz, B. H. & Ghorai, S. Transitioning organic synthesis from organic solvents to water. What's your E Factor? *Green Chem.* **16**, 3660-3679, (2014).

18 Lipshutz, B. H., Gallou, F. & Handa, S. Evolution of Solvents in Organic Chemistry. *ACS Sustainable Chem. Eng.* **4**, 5838-5849, (2016).

19 Bella, F., Gerbaldi, C., Barolo, C. & Grätzel, M. Aqueous dye-sensitized solar cells. *Chem. Soc. Rev.* **44**, 3431-3473, (2015).

20 Mariotti, N. *et al.* Recent advances in eco-friendly and cost-effective materials towards sustainable dye-sensitized solar cells. *Green Chem.* **22**, 7168-7218, (2020).

21 Bella, F. *et al.* A water-based and metal-free dye solar cell exceeding 7% efficiency using a cationic poly(3,4-ethylenedioxythiophene) derivative. *Chem. Sci.* **11**, 1485-1493, (2020).

22 Galliano, S. *et al.* Photoanode/Electrolyte Interface Stability in Aqueous Dye-Sensitized Solar Cells. *Energy Technol.* **5**, 300-311, (2017).

23 Kim, J.-H., Kim, D.-H., So, J.-H. & Koo, H.-J. Toward Eco-Friendly Dye-Sensitized Solar Cells (DSSCs): Natural Dyes and Aqueous Electrolytes. *Energies* **15**, 219, (2022).

24 Sayah, D. & Ghaddar, T. H. Copper-Based Aqueous Dye-Sensitized Solar Cell: Seeking a Sustainable and Long-Term Stable Device. *ACS Sustainable Chem. Eng.* **12**, 6424-6432, (2024).

25 Hansen, B. B. *et al.* Deep Eutectic Solvents: A Review of Fundamentals and Applications. *Chem. Rev.* **121**, 1232-1285, (2021).

26 Jhong, H.-R., Wong, D. S.-H., Wan, C.-C., Wang, Y.-Y. & Wei, T.-C. A novel deep eutectic solvent-based ionic liquid used as electrolyte for dye-sensitized solar cells. *Electrochem. Commun.* **11**, 209-211, (2009).

27 Boldrini, C. L. *et al.* Dye-Sensitized Solar Cells that use an Aqueous Choline Chloride-Based Deep Eutectic Solvent as Effective Electrolyte Solution. *Energy Technol.* **5**, 345-353, (2017).

28 Boldrini, C. L., Quivelli, A. F., Manfredi, N., Capriati, V. & Abbotto, A. Deep Eutectic Solvents in Solar Energy Technologies. *Molecules* **27**, 709, (2022).

29 Nguyen, D. *et al.* Urea–acetamide-based deep eutectic compound as novel, eco-friendly additives in stable and efficient dye-sensitized solar cells: A performance and electrochemical study. *Electrochim. Acta* **487**, 144156, (2024).

30 Nguyen, D. *et al.* Choline chloride-based deep eutectic solvents as effective electrolytes for dye-sensitized solar cells. *RSC Adv.* **11**, 21560-21566, (2021).

31 Das, S. & Mao, E. The global energy footprint of information and communication technology electronics in connected Internet-of-Things devices. *SEGAN* **24**, 100408, (2020).

32 Ren, Y. *et al.* Hydroxamic acid pre-adsorption raises the efficiency of cosensitized solar cells. *Nat.* **613**, 60-65, (2023).

33 Devadiga, D., Selvakumar, M., Shetty, P. & Santosh, M. S. Dye-Sensitized Solar Cell for Indoor Applications: A Mini-Review. *J. Electron. Mater.* **50**, 3187-3206, (2021).

34 Michaels, H. *et al.* Dye-sensitized solar cells under ambient light powering machine learning: towards autonomous smart sensors for the internet of things. *Chem. Sci.* **11**, 2895-2906, (2020).

35 Jagadeesh, A., Veerappan, G., Devi, P. S., Unni, K. N. N. & Soman, S. Synergetic effect of TiO_2/ZnO bilayer photoanodes realizing exceptionally high VOC for dye-sensitized solar cells under outdoor and indoor illumination. *J. Mater. Chem. A* **11**, 14748-14759, (2023).

36 Pecunia, V., Occhipinti, L. G. & Hoye, R. L. Z. Emerging Indoor Photovoltaic Technologies for Sustainable Internet of Things. *Adv. Energy Mater.* **11**, 2100698, (2021).

37 Devadiga, D., Selvakumar, M., Shetty, P. & Santosh, M. S. The integration of flexible dye-sensitized solar cells and storage devices towards wearable self-charging power systems: A review. *Renew. Sustain. Energy Rev.* **159**, 112252, (2022).

38 Pulli, E., Rozzi, E. & Bella, F. Transparent photovoltaic technologies: Current trends towards upscaling. *Energy Convers. Manage.* **219**, 112982, (2020).

39 Salerno, G. *et al.* Optimizing DSSCs Performance for Indoor Lighting: Matching Organic Dyes Absorption and Indoor Lamps Emission Profiles to Maximize Efficiency. *ChemistryOpen* **14**, e202400464, (2025).

40 Marrugat-Arnal V. *et al.* Tuning $FAPbI_3$ for scalable perovskite indoor photovoltaics. *EES Sol.*, **1**, 310, (2025).

41 Xu J. *et al.* Triple-halide wide–band gap perovskites with suppressed phase segregation for efficient tandems. *Science* **367**, 1097–1104, (2020).

42 Xiao K. *et al*. Scalable processing for realizing 21.7%-efficient all-perovskite tandem solar modules. *Science* **376**, 762–767, (2022).

43 Siegris S. *et al.* Unveiling the Role of Cl Incorporation Enables Scalable MA-Free Triple-Halide Wide-Bandgap Perovskitesfor Slot-Die-Coated Photovoltaic Modules. *Sol. RRL,* **9**, 2400750, (2025).

44 Wang *et al.* High-performance organic photovoltaic cells under indoor lighting enabled by suppressing energetic disorders. *Joule* **7**, 1067–1079, (2023).

45 Michaels, H. et al. Emerging indoor photovoltaics for self-powered and self-aware IoT towards sustainable energy management. *Chem. Sci.* 14, 5350-5360, (2023).

46 Boldrini, C. L. *et al.* Top-ranked efficiency under indoor light of DSSCs enabled by iodide-based DES-like solvent electrolyte. *Sustain. Energ. Fuels* **8**, 504-515, (2024).

47 Mauri, L., Colombo, A., Dragonetti, C., Roberto, D. & Fagnani, F. Recent Investigations on Thiocyanate-Free Ruthenium(II) 2,2′-Bipyridyl Complexes for Dye-Sensitized Solar Cells. *Molecules* **26**, 7638, (2021).

48 Dragonetti, C. *et al.* A new thiocyanate-free cyclometallated ruthenium complex for dye-sensitized solar cells: Beneficial effects of substitution on the cyclometallated ligand. *J. Organomet. Chem.* **714**, 88-93, (2012).

49 Manfredi, N. *et al.* Enhanced photocatalytic hydrogen generation using carbazole-based sensitizers. *Sustain. Energ. Fuels* **1**, 694-698, (2017).

50 Wu, W. *et al.* Structure−Activity Relationships in Toll-like Receptor-2 Agonistic Diacylthioglycerol Lipopeptides. *J. Med. Chem.* **53**, 3198-3213, (2010).

51 Davies, S. G. *et al.* On the origins of diastereoselectivity in the conjugate additions of the antipodes of lithium N-benzyl-(N-α-methylbenzyl)amide to enantiopure cis- and trans-dioxolane containing α,β-unsaturated esters. *Org. Biomol. Chem.* **10**, 6186-6200, (2012).

52 Majchrzak, M., Grzelak, M. & Marciniec, B. Synthesis of novel styryl-N-isopropyl-9H-carbazoles for designing trans-conjugated regular silicon hybrid materials. *Org. Biomol. Chem.* **14**, 9406-9415, (2016).

53 Manfredi, N., Cecconi, B. & Abbotto, A. Multi-Branched Multi-Anchoring Metal-Free Dyes for Dye-Sensitized Solar Cells. *Eur. J. Org. Chem.* **2014**, 7069-7086, (2014).

54 Zhang, L. & Cole, J. M. Dye aggregation in dye-sensitized solar cells. *J. Mater. Chem. A* **5**, 19541-19559, (2017).

55 Tauc, J. Optical properties and electronic structure of amorphous Ge and Si. *Mater. Res. Bull.* **3**, 37-46, (1968).

56. Grisorio R. *et al.* Anchoring stability and photovoltaic properties of new D(-π-A)2 dyes for dye-sensitized solar cell applications. *Dyes Pigm.* **98**, 221-231, (2013)

57. Gupta K.S.V. *et al.* Carbazole based A-p-D-p-A dyes with double electron acceptor for dye-sensitized solar cell. *Org. Electron.* **15**, 266–275, (2014)

58 Manfredi, N. *et al.* Performance enhancement of a dye-sensitized solar cell by peripheral aromatic and heteroaromatic functionalization in di-branched organic sensitizers. *New J. Chem.* **42**, 9281-9290, (2018).

59 Fabregat-Santiago, F., Garcia-Belmonte, G., Mora-Seró, I. & Bisquert, J. Characterization of nanostructured hybrid and organic solar cells by impedance spectroscopy. *Phys. Chem. Chem. Phys.* **13**, 9083-9118, (2011).

60 Sacco, A. Electrochemical impedance spectroscopy: Fundamentals and application in dye-sensitized solar cells. *Renew. Sustain. Energy Rev.* **79**, 814-829, (2017).

61 Heydari Dokoohaki, M., Mohammadpour, F. & Zolghadr, A. R. Dye-Sensitized Solar Cells Based on Deep Eutectic Solvent Electrolytes: Insights from Experiment and Simulation. *J. Phys. Chem. C* **125**, 15155-15165, (2021).

62 Boldrini, C. L., Manfredi, N., Perna, F. M., Capriati, V. & Abbotto, A. Eco-Friendly Sugar-Based Natural Deep Eutectic Solvents as Effective Electrolyte Solutions for Dye-Sensitized Solar Cells. *ChemElectroChem* **7**, 1707-1712, (2020).

63 Lu, H.-L., Shen, T. F. R., Huang, S.-T., Tung, Y.-L. & Yang, T. C. K. The degradation of dye sensitized solar cell in the presence of water isotopes. *Sol. Energy Mater. Sol. Cells* **95**, 1624-1629, (2011).

64 Ronca, E., Pastore, M., Belpassi, L., Tarantelli, F. & De Angelis, F. Influence of the dye molecular structure on the TiO2 conduction band in dye-sensitized solar cells: disentangling charge transfer and electrostatic effects. *Energy Environ. Sci.* **6**, 183-193, (2013).

65 Prabavathy, N. *et al.* Enhancement in the photostability of natural dyes for dye-sensitized solar cell (DSSC) applications: a review. *IJER* **41**, 1372-1396, (2017).

66 Ito, S. *et al.* Fabrication of thin film dye sensitized solar cells with solar to electric power conversion efficiency over 10%. *Thin Solid Films* **516**, 4613-4619, (2008).

67 Chen, C. *et al.* PEDOT-based counter electrodes for dye-sensitized solar cells: rigid, flexible and indoor light applications. *Mater. Chem. Front.* **8**, 3413-3445, (2024).

68 Bella, F. *et al.* Unveiling iodine-based electrolytes chemistry in aqueous dye-sensitized solar cells. *Chem. Sci.* **7**, 4880-4890, (2016).

69 Bella, F. *et al.* Boosting the efficiency of aqueous solar cells: A photoelectrochemical estimation on the effectiveness of TiCl4 treatment. *Electrochim. Acta* **302**, 31-37, (2019).

Acknowledgements

The authors thank the Ministero dell'Università e della Ricerca (PRIN2022 Mendeleev, Project no.2022KMS84P funded by European Union - NextGenerationEU, Piano Nazionale di Ripresa e Resilienza (PNRR) M4 C2 I.1.1 CUP H53D23004590006), Ministero dell'Ambiente e della Sicurezza Energetica (SOLE-H2, Project RSH2A_000004 - CUP: F57G25000080006, funded by European Union - NextGenerationEU, Piano Nazionale di Ripresa e Resilienza (PNRR) Missione 2 Componente 2 Investimento 3.5 - D.D. 279 05/08/2025, and Sustainable Mobility Center (CNMS-MOST) funded by European Union - NextGenerationEU, Piano Nazionale di Ripresa e Resilienza (PNRR) Missione 4 Componente 2, Investimento 1.4 – D.D. 1033 17/06/2022, CN00000023) for financial support. Open Access publishing facilitated by Università degli Studi di Milano-Bicocca, as part of the Wiley - CRUI-CARE agreement

Author contributions

G.S. and O.B. synthesized and characterized the dyes. G.S. and C.B investigated the solar cells by EIS and performed the IPCE measurements. G.S., O.B. and C.B. fabricated, optimized and characterized the solar cells. N.M. supported the photovoltaic data analysis. V.C. supported the DES data interpretation. A.A. and O.B. conceived the main conceptual idea, conceived and planned the experiments, interpreted the results and wrote the manuscript, with contributions from all authors. All authors have given approval to the final version of the manuscript.

Competing interests.

The authors declare no competing interests

678

679 **Scheme 1.** Synthetic route for the synthesis of dyes CBZ-EG and CBZ-Gly

680

681 **Figure 1. Structures of the CBZ-dyes.** Two original dyes investigated in this work, CBZ-EG and
682 CBZ-Gly, and the reference dye CBZ-Alk.

683

684 **Figure 2. *J/V* curves (1 sun, AM 1.5G) of CBZ-EG, CBZ-Gly, and CBZ-Alk sensitized DSSCs.**
685 a) *J/V* curves using ChCl:EG as a DES electrolyte (blue panel); b) *J/V* curves using ChCl:Gly as a
686 DES electrolyte (green panel).

687 **Figure 3. IPCE curves of CBZ-dyes sensitized DSSCs.** a) IPCE curves of CBZ-EG, CBZ-Gly, and
688 CBZ-Alk sensitized DSSCs using ChCl:EG as a DES electrolyte (blue panel); b) IPCE curves of
689 CBZ-EG, CBZ-Gly, and CBZ-Alk sensitized DSSCs using ChCl:Gly as a DES electrolyte (green
690 panel).

691 **Figure 4. Nyquist plots from EIS measurements under 0.23 sun illumination (AM1.5G).** a)
692 CBZ-EG, CBZ-Gly, and CBZ-Alk sensitized DSSCs using ChCl:EG as a DES electrolyte (blue
693 panel); b) CBZ-EG, CBZ-Gly, and CBZ-Alk sensitized DSSCs using ChCl:Gly as a DES electrolyte.
694 Lines represent the fitting according to the equivalent circuit in the inset.

695

696 **Figure 5. Stability test of DSSCs sensitized by CBZ-based dyes in a ChCl:Gly DES electrolyte**.
697 a) PCE (i) and J_{sc} (ii) variation over 120 days; b) *J/V* curves of DSSCs (1 sun, AM 1.5G) of the three
698 dyes at day 1 and at day 120.
699

700 **Figure 6. *J/V* curves and stability test of DSSCs sensitized by CBZ-based dyes (1 sun, AM**
701 **1.5G) using neat and aqueous DES electrolytes**. a) *J/V* curves obtained using neat ChCl:Gly
702 as the DES electrolyte (dotted lines) compared with those recorded using ChCl:Gly diluted with
703 40% H_2O as the electrolyte (solid lines); b) Stability test of DSSCs main PV characteristics, PCE
704 (i) and J_{sc} (ii) over 30 days.

705

706 **Table 1.** *J/V* characteristics of DSSCs sensitized by dyes CBZ-EG CBZ-Gly, and CBZ-Alk in two
707 DES electrolytes (ChCl:EG and ChCl:Gly) under AM 1.5G sun-simulated light.

DES	Dye	J_{sc} (mA cm^{-2})	V_{oc} (mV)	FF	PCE (%)
ChCl:EG	CBZ-EG	8.0	466	0.56	2.0
		(7.7 ± 0.9)	(460 ± 20)	(0.57 ± 0.04)	(1.9 ± 0.1)
	CBZ-Gly	5.7	452	0.64	1.7
		(5.7 ±0.5)	(430 ± 40)	(0.54 ± 0.09)	(1.3 ± 0.3)
	CBZ-Alk	5.2	371	0.48	0.9
		(4.3 ± 0.9)	(400 ± 60)	(0.50 ± 0.03)	(0.8 ± 0.1)
ChCl:Gly	CBZ-EG	6.3	487	0.50	1.6
		(5.5 ± 0.7)	(490 ± 10)	(0.49 ± 0.02)	(1.3 ± 0.2)
	CBZ-Gly	9.6	533	0.59	3.0
		(9.3 ± 0.4)	(500 ± 30)	(0.56 ± 0.25)	(2.6 ± 0.3)

	CBZ-Alk	3.5 (3.1 ± 0.4)	398 (400 ± 10)	0.51 (0.53 ± 0.03)	0.7 (0.6 ± 0.1)

Average values over 3 devices in parentheses.

Table 3. *J/V* characteristics under AM 1.5G sun-simulated light of DSSCs sensitized by dyes CBZ-EG, CBZ-Gly, and CBZ-Alk in ChCl:Gly diluted in 40% H_2O.

DES	Dye	J_{sc} (mA cm^{-2})	V_{oc} (mV)	FF	PCE (%)
ChCl:Gly 40% H_2O	CBZ-EG	5.1 (5.0 ± 0.2)	457 (450 ± 10)	0.59 (0.49 ± 0.09)	1.5 (1.1 ± 0.3)
	CBZ-Gly	4.0 (4.2 ± 0.4)	415 (410 ± 10)	0.55 (0.53 ± 0.03)	0.9 (0.9 ± 0.1)
	CBZ-Alk	4.3 (5.2 ± 0.8)	478 (430 ± 40)	0.53 (0.45 ± 0.07)	1.0 (1.0 ± 0.1)

Average values over 3 devices in parentheses.

Table 4. PCE values of CBZ-DSSCs under OSRAM 765 and OSRAM 930 illumination (1000 lux) filled with the two DES electrolytes investigated (ChCl:EG and ChCl:Gly).

DES	Dye	PCE (%)	
		OSRAM 765	OSRAM 930
ChCl:EG	CBZ-EG	6.1 (6.0 ± 0.1)	4.8 (4.5 ± 0.4)
	CBZ-Gly	3.6 (3.5 ± 0.1)	3.3 (2.5 ± 0.6)
	CBZ-Alk	4.0 (3.2 ± 0.7)	3.9 (2.3 ± 1.1)
ChCl:Gly	CBZ-EG	8.4 (8.0 ± 0.4)	5.8 (5.4 ± 0.3)
	CBZ-Gly	9.4 (8.7 ± 0.9)	6.5 (6.4 ± 0.1)
	CBZ-Alk	4.6 (4.5 ± 0.1)	5.3 (5.2 ± 0.1)

Average values over 3 devices in parentheses

Table 2. Recombination resistance (R_{rec}), chemical capacitance (C_μ) and electron lifetimes (τ_n) obtained from Nyquist plot data fitting of the investigated DSSC.

DES	Dye	R_{rec} (Ω)	C_μ (μF)	τ_n (ms)
ChCl:EG	CBZ-EG	119.3 ± 1.6	41.3 ± 2.5	4.9 ± 0.4
	CBZ-Gly	113.4 ± 1.2	41.7 ± 1.0	4.7 ± 0.2
	CBZ-Alk	85.9 ± 0.8	42.8 ± 1.3	3.7 ± 0.1

	CBZ-EG	111.5 ± 0.9	76.1 ± 1.4	8.5 ± 0.2
ChCl:Gly	CBZ-Gly	171.2 ± 2.1	66.3 ± 3.8	11.4 ± 0.8
	CBZ-Alk	101.1 ± 0.4	75.0 ± 1.0	7.6 ± 0.1

Values obtained under AM1.5G 0.23 sun irradiation.

708
709
710
711
712
713
714

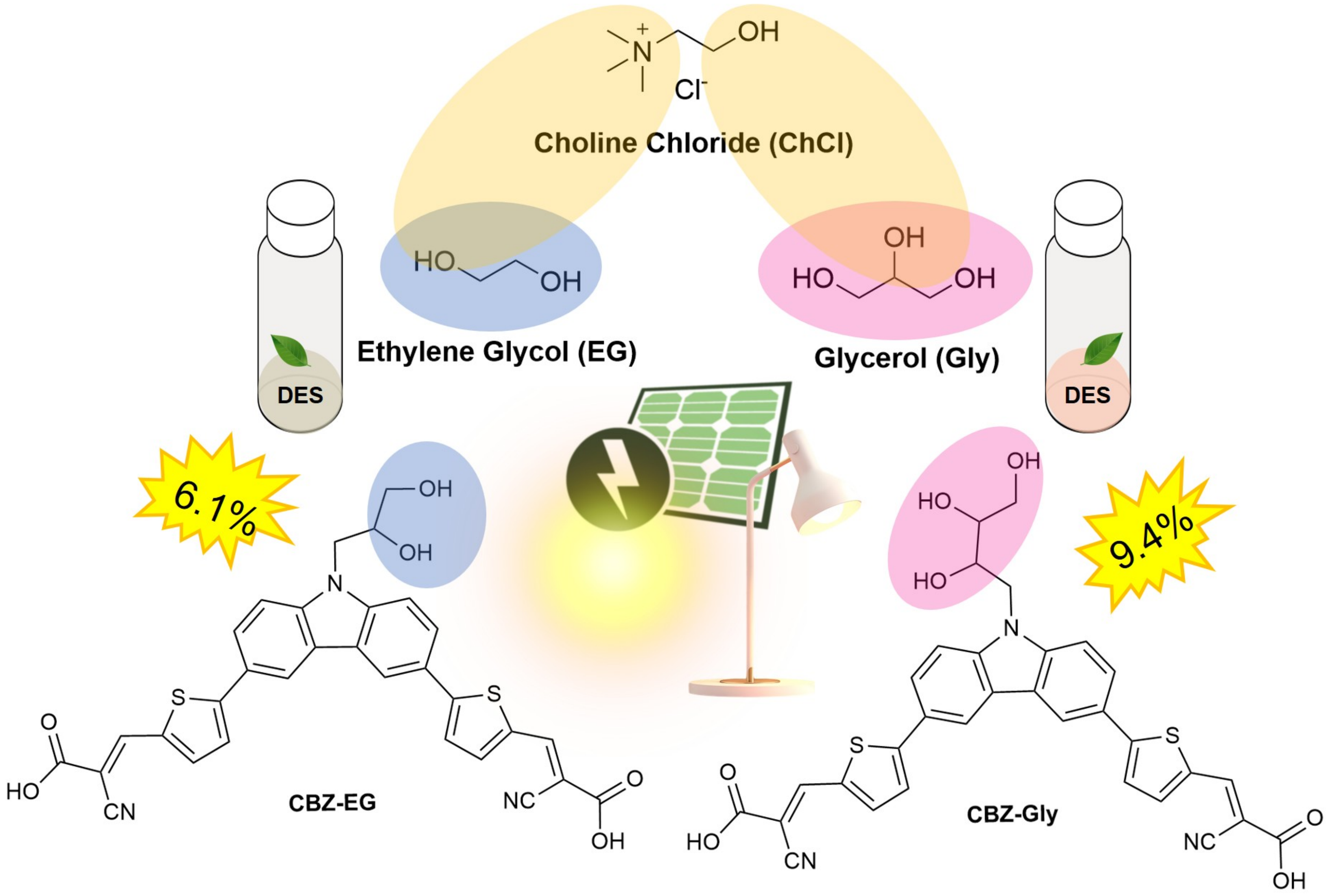
Choline Chloride (ChCl)
Ethylene Glycol (EG)
Glycerol (Gly)
DES
DES
6.1%
9.4%
CBZ-EG
CBZ-Gly

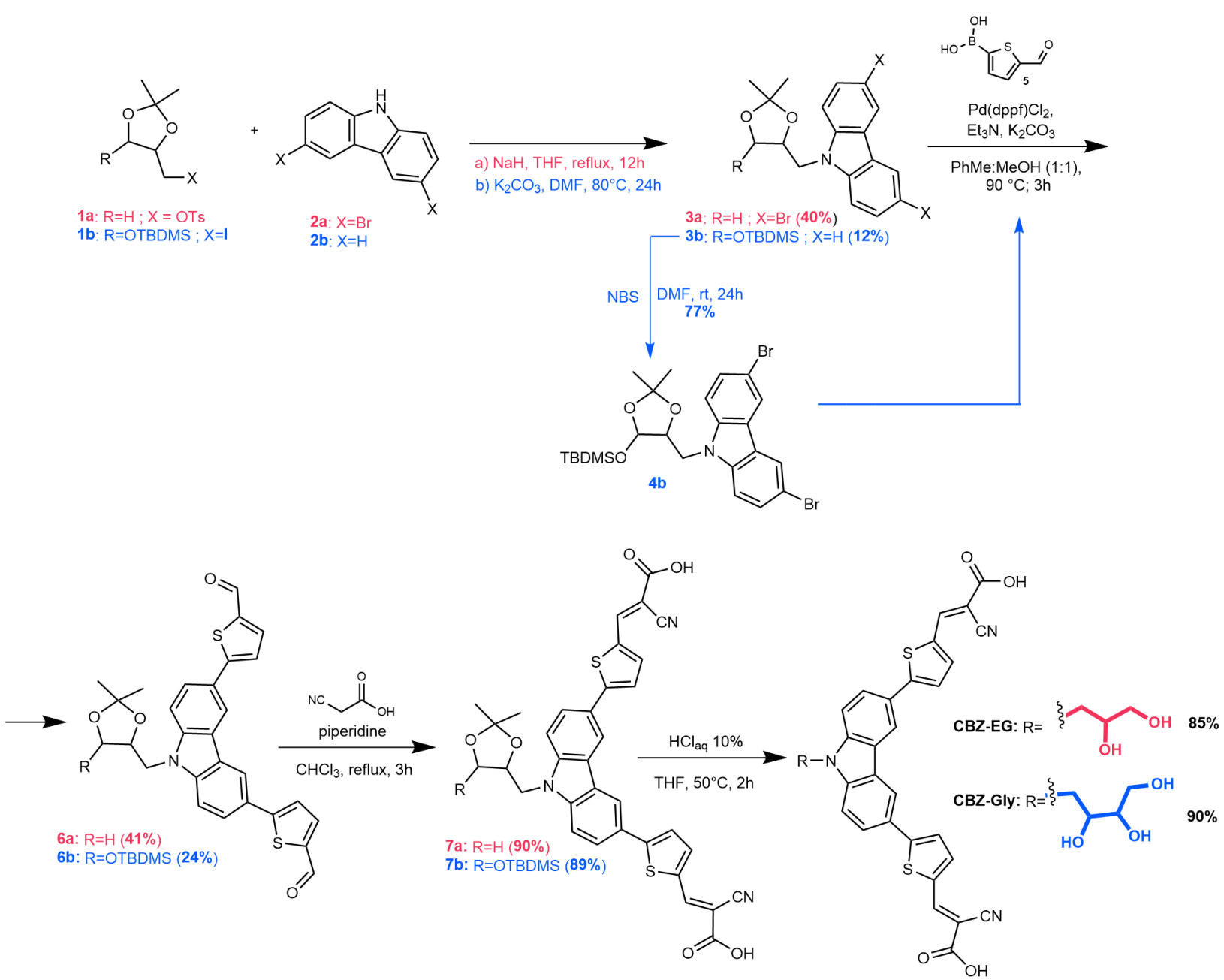
1a: R=H ; X = OTs
1b: R=OTBDMS ; X=I
2a: X=Br
2b: X=H
a) NaH, THF, reflux, 12h
b) K2CO3, DMF, 80°C, 24h
3a: R=H ; X=Br (40%)
3b: R=OTBDMS ; X=H (12%)
5
Pd(dppf)Cl2,
Et3N, K2CO3
PhMe:MeOH (1:1),
90 °C; 3h
NBS
DMF, rt, 24h
77%
4b
6a: R=H (41%)
6b: R=OTBDMS (24%)
piperidine
CHCl3, reflux, 3h
7a: R=H (90%)
7b: R=OTBDMS (89%)
HClaq 10%
THF, 50°C, 2h
CBZ-EG: R=
85%
CBZ-Gly: R=
90%

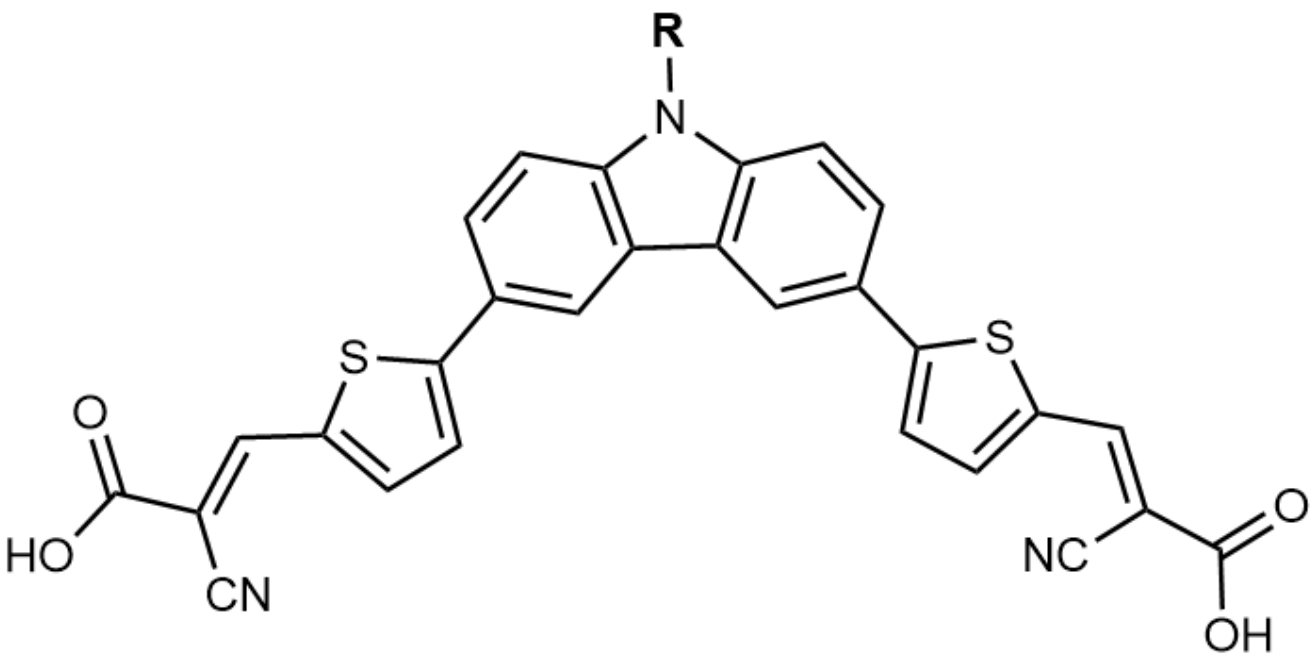

R:

CBZ-Alk

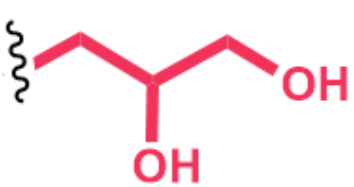

CBZ-EG

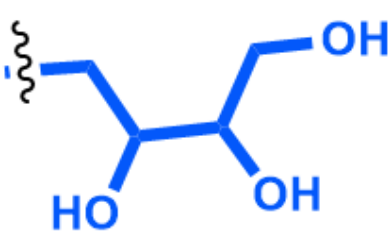

CBZ-Gly

AM 1.5 G

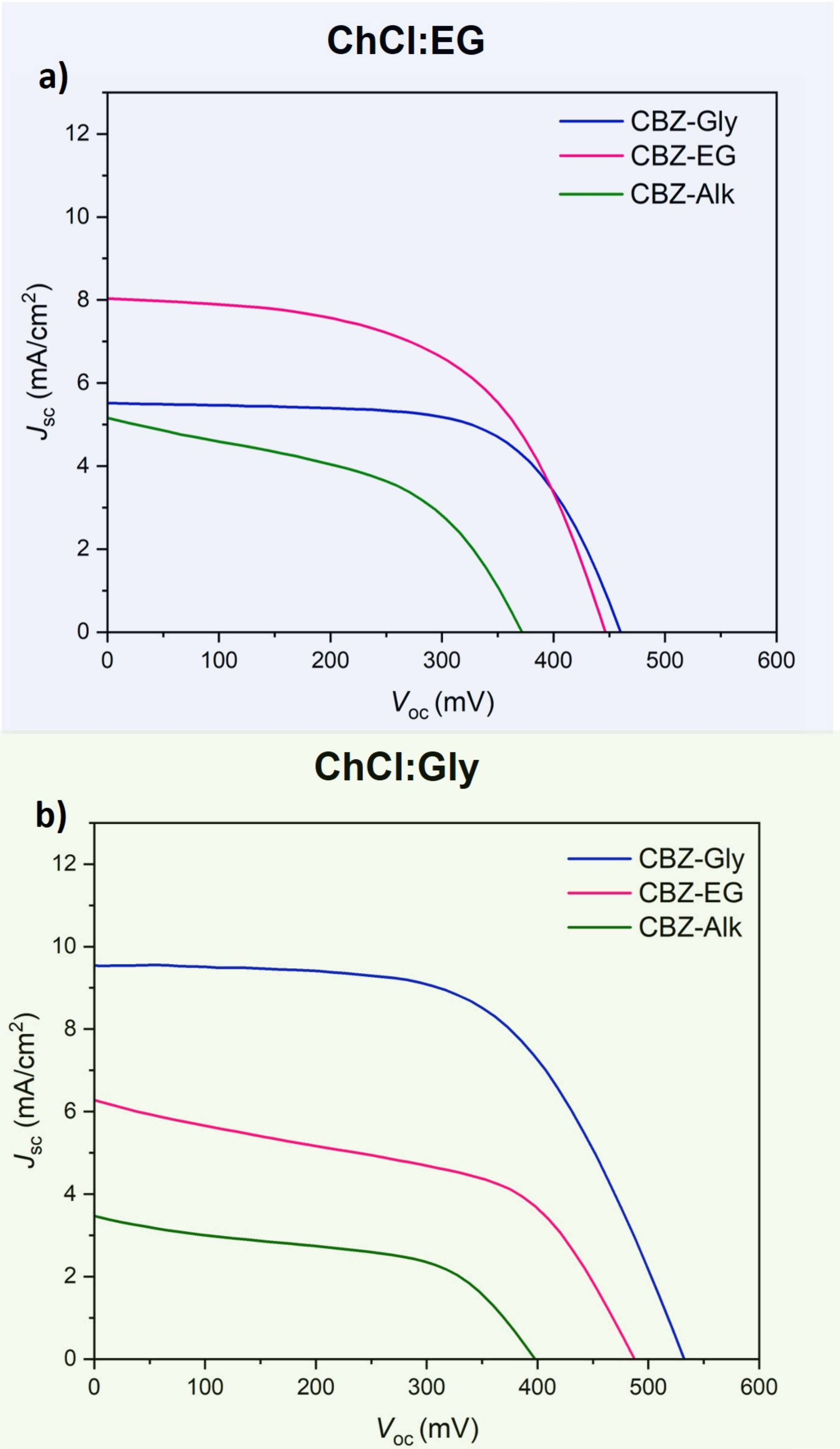
ChCl:EG
a)
CBZ-Gly
CBZ-EG
CBZ-Alk
J_{sc} (mA/cm^2)
V_{oc} (mV)
0
2
4
6
8
10
12
0
100
200
300
400
500
600
ChCl:Gly
b)
CBZ-Gly
CBZ-EG
CBZ-Alk
J_{sc} (mA/cm^2)
V_{oc} (mV)

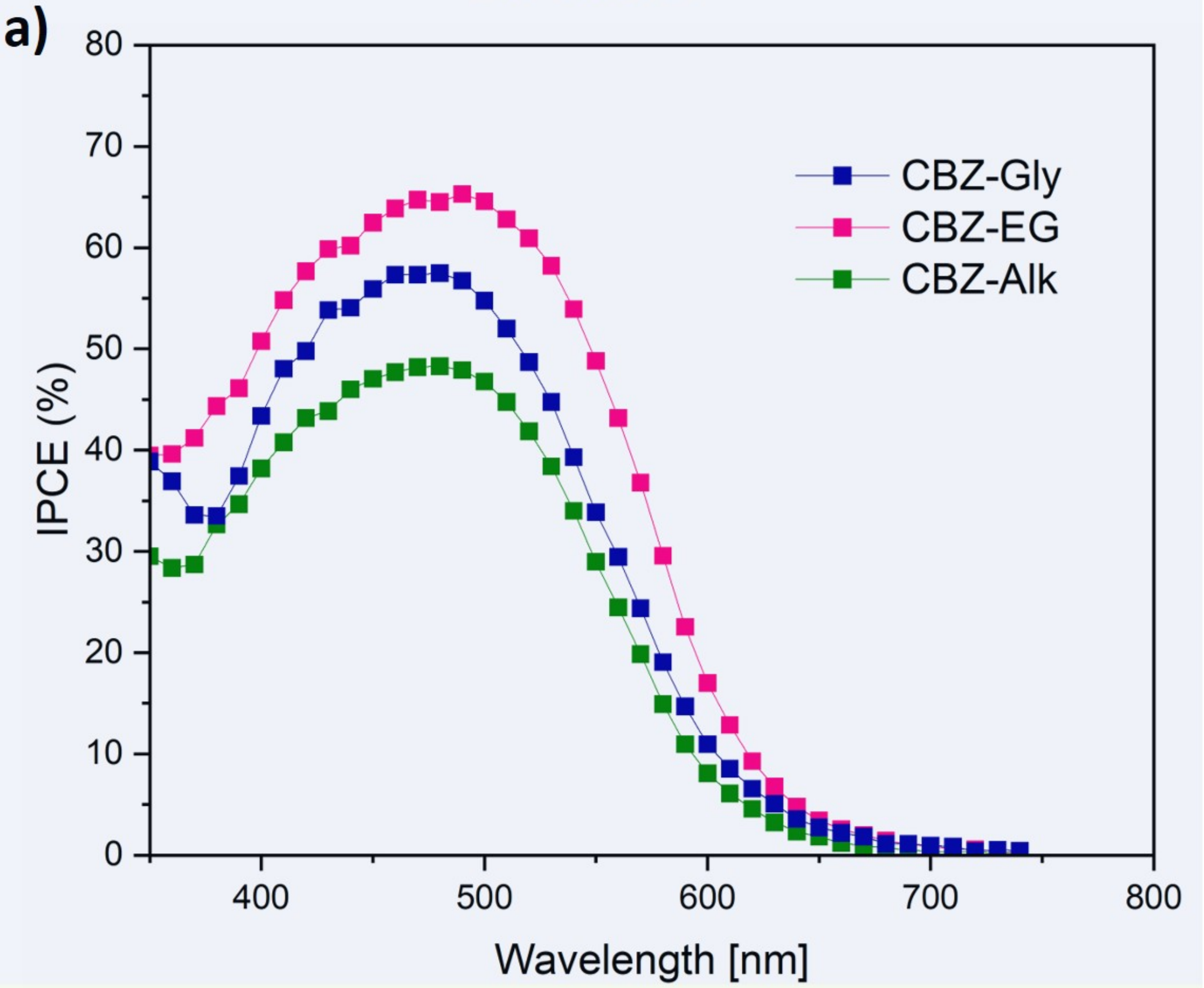
ChCl:EG
a)
IPCE (%)
Wavelength [nm]
CBZ-Gly
CBZ-EG
CBZ-Alk
ChCl:Gly
b)
IPCE (%)
Wavelength (nm)
CBZ-Gly
CBZ-EG
CBZ-Alk

a)

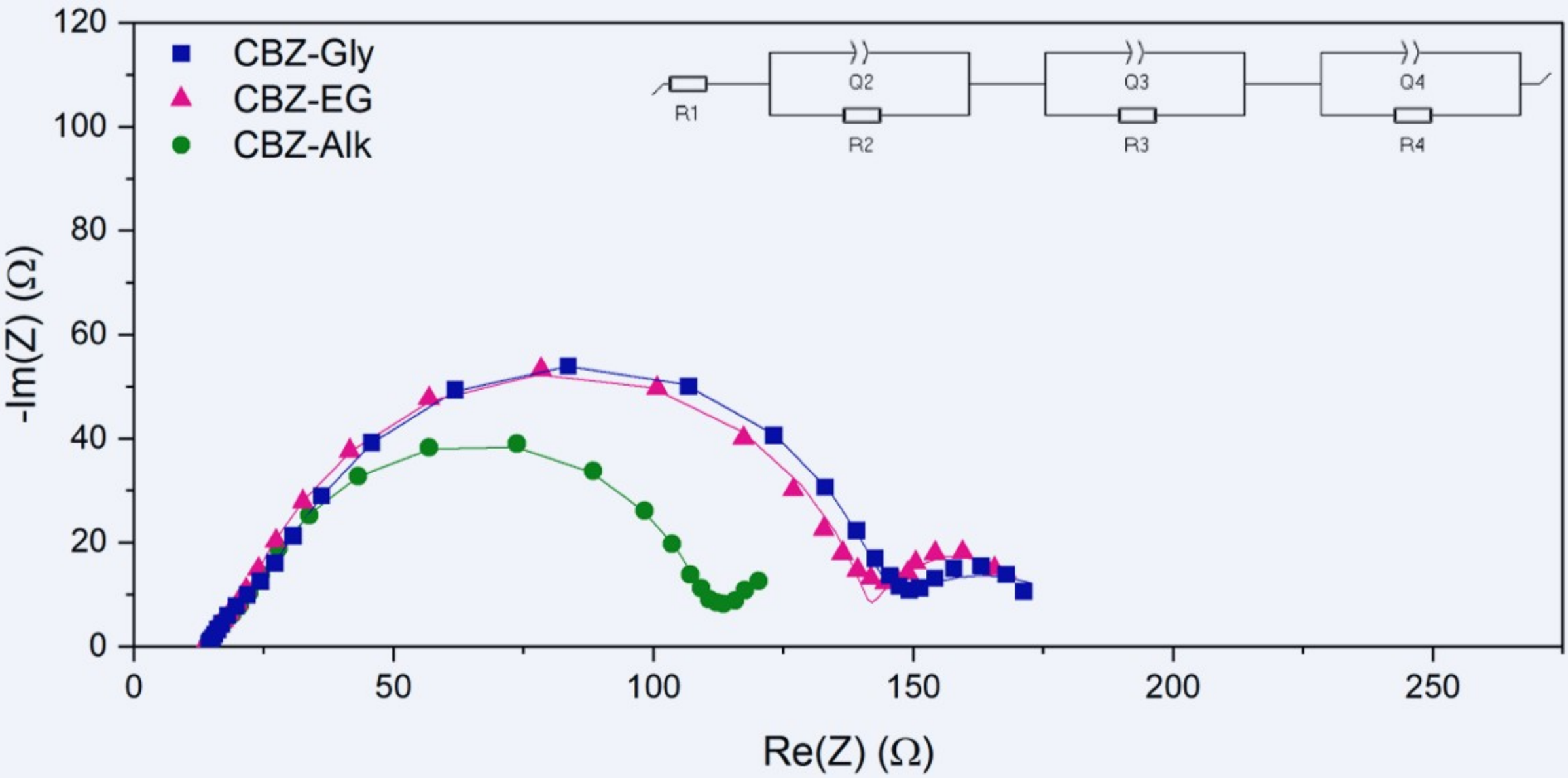
ChCl:EG
CBZ-Gly
CBZ-EG
CBZ-Alk
R1
Q2
R2
Q3
R3
Q4
R4
-Im(Z) (Ω)
Re(Z) (Ω)
0
20
40
60
80
100
120
0
50
100
150
200
250

b)

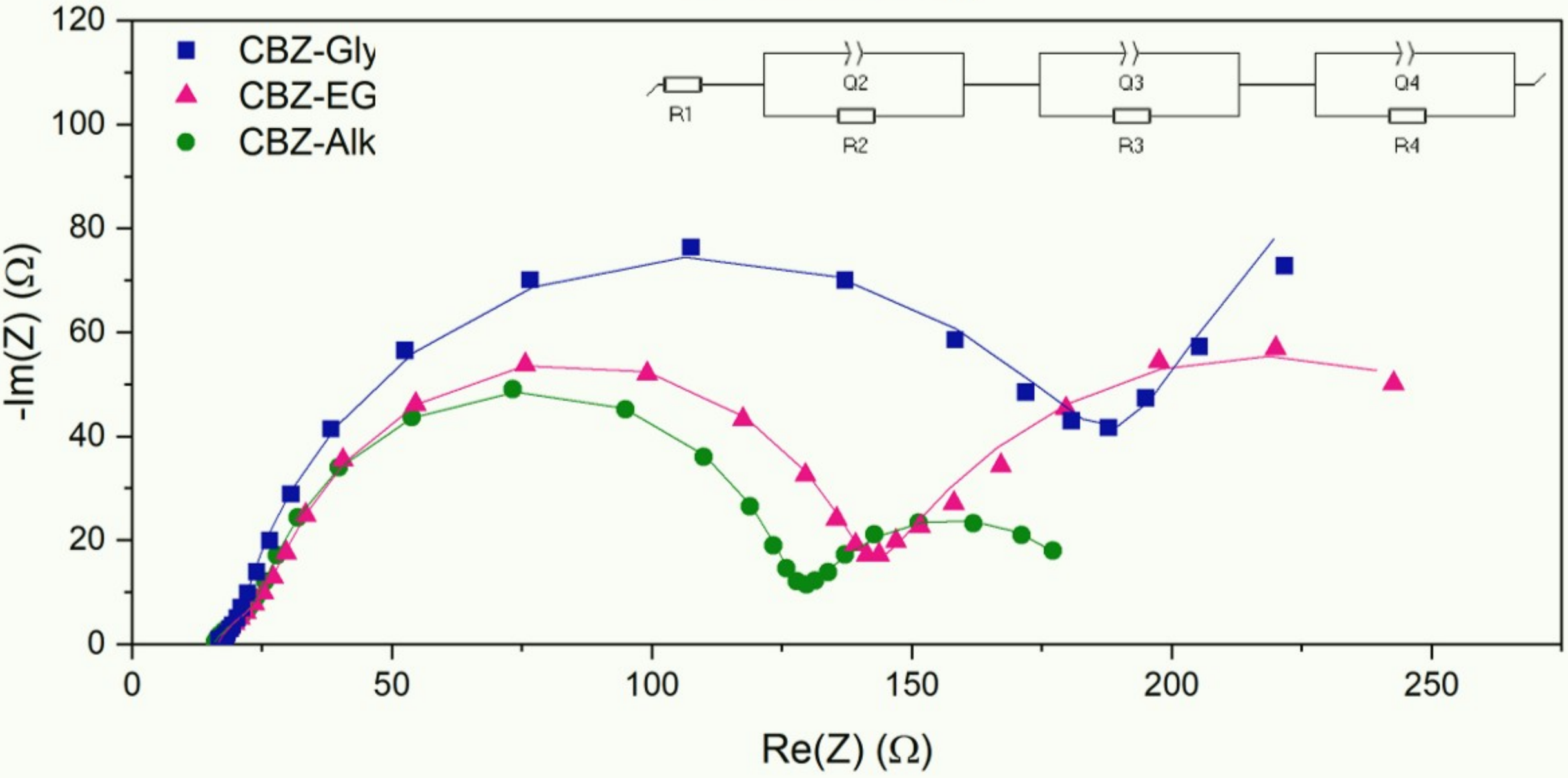
ChCl:Gly
CBZ-Gly
CBZ-EG
CBZ-Alk
R1
Q2
R2
Q3
R3
Q4
R4
-Im(Z) (Ω)
Re(Z) (Ω)
0
20
40
60
80
100
120
0
50
100
150
200
250

Stability test (AM 1.5 G)

ChCl:Gly

a)

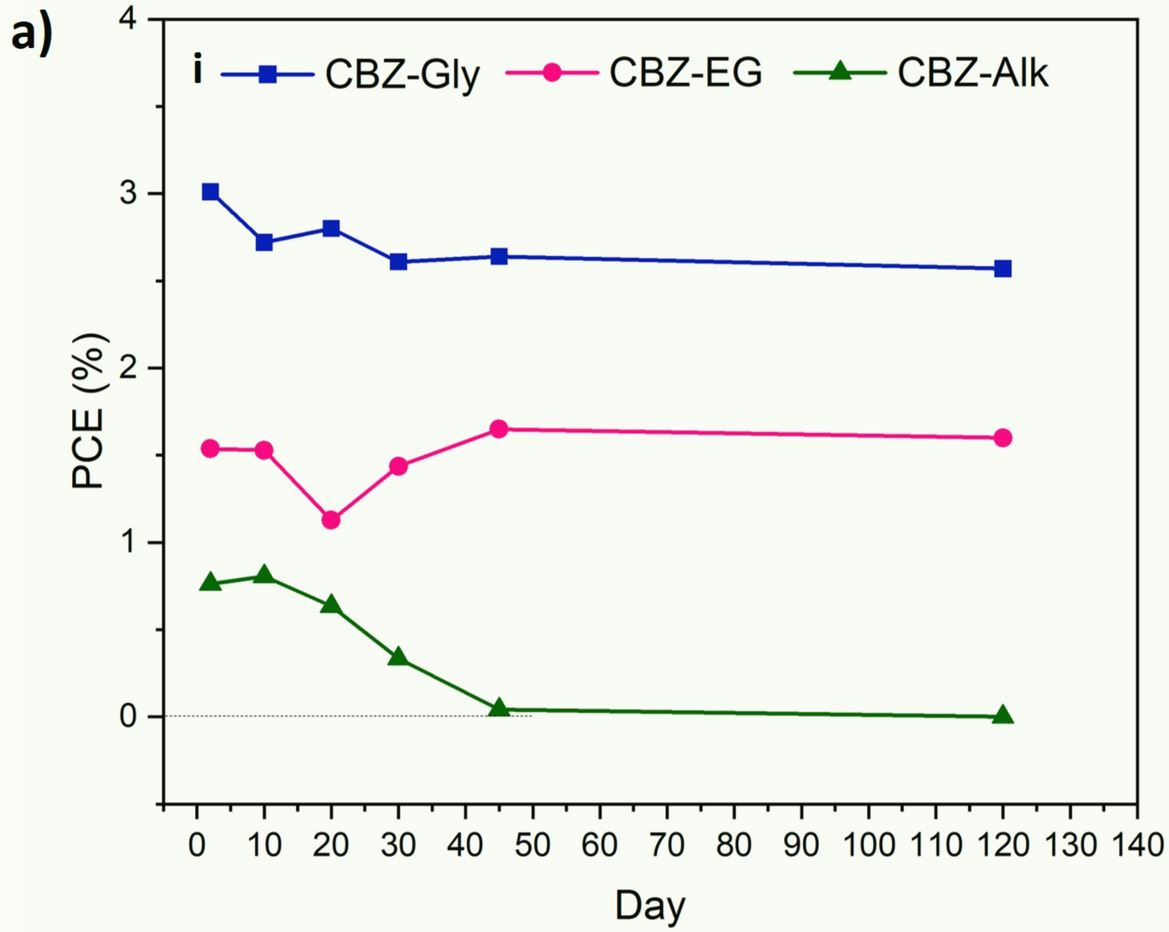

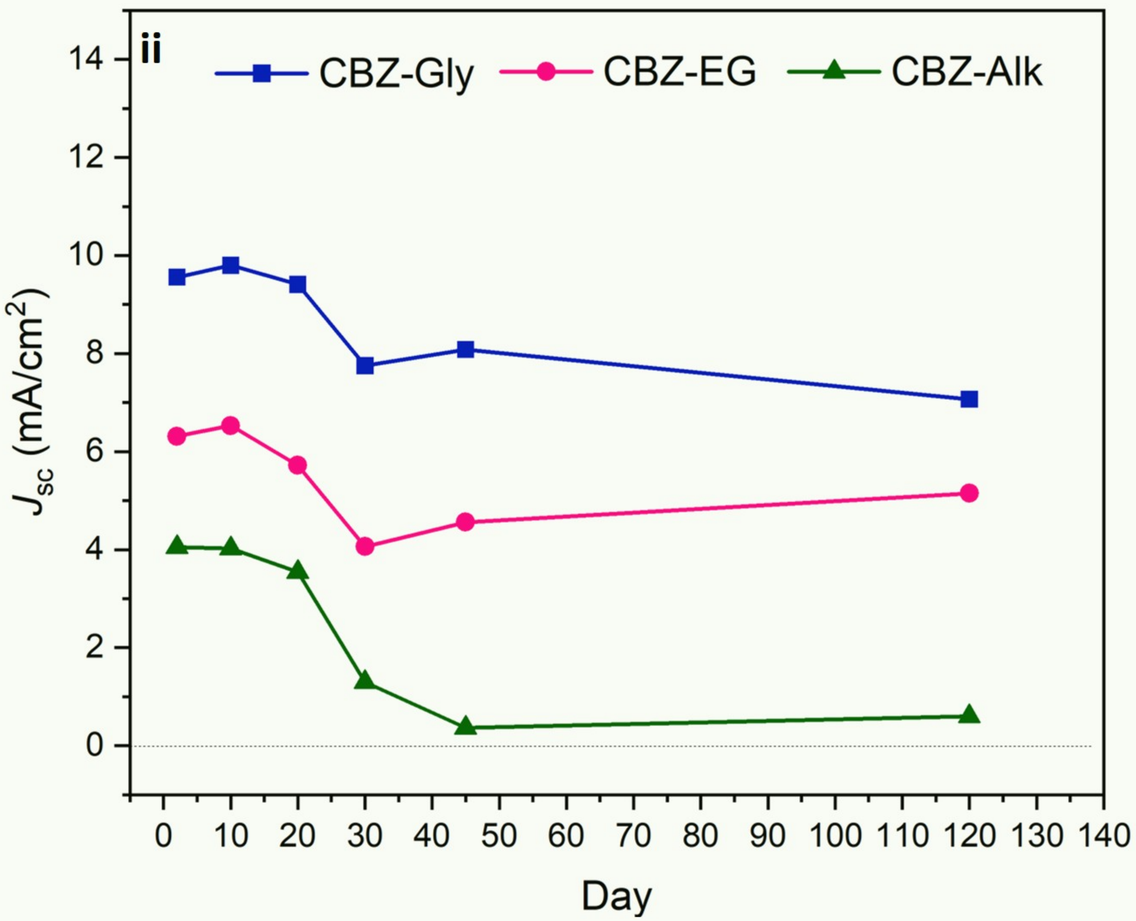

b)

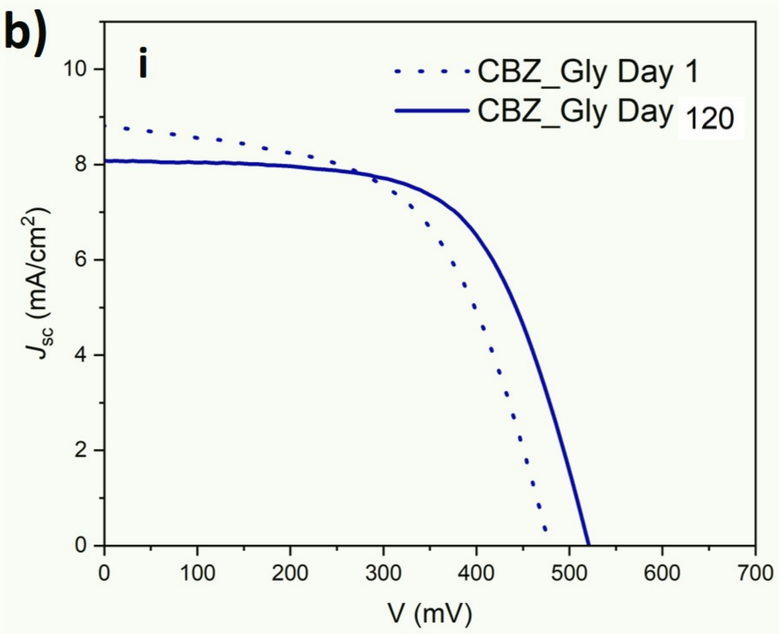

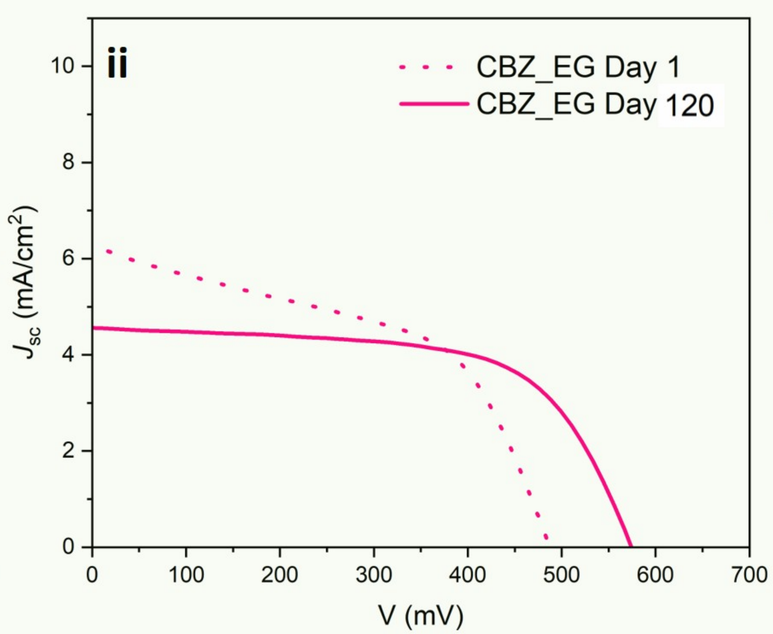

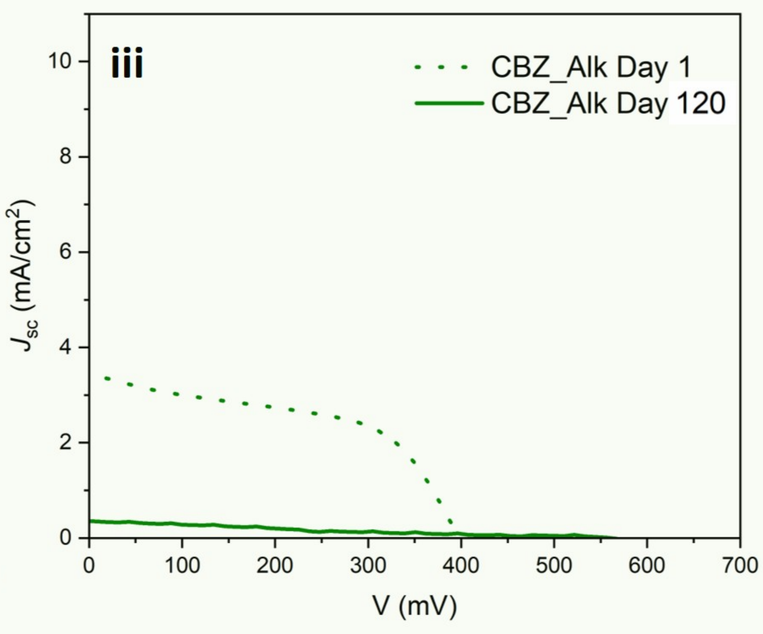

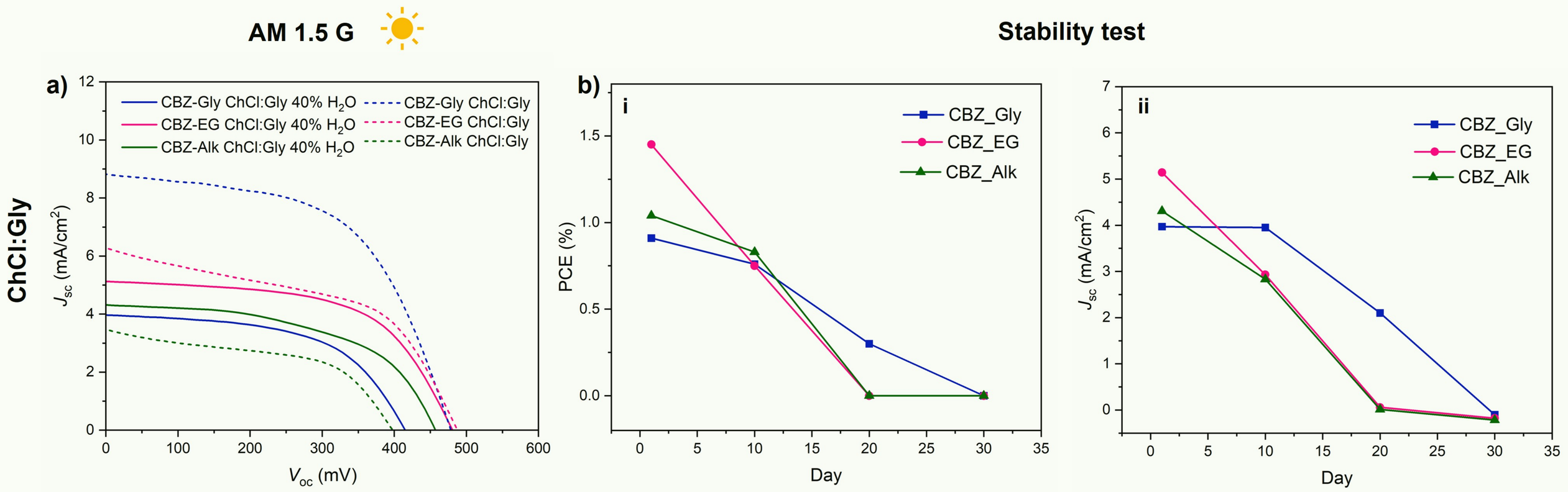
AM 1.5 G
Stability test
ChCl:Gly
a)
CBZ-Gly ChCl:Gly 40% H2O
CBZ-EG ChCl:Gly 40% H2O
CBZ-Alk ChCl:Gly 40% H2O
CBZ-Gly ChCl:Gly
CBZ-EG ChCl:Gly
CBZ-Alk ChCl:Gly
Jsc (mA/cm2)
Voc (mV)
b)
i
PCE (%)
Day
CBZ_Gly
CBZ_EG
CBZ_Alk
ii
Jsc (mA/cm2)
Day
CBZ_Gly
CBZ_EG
CBZ_Alk